frontiers in Environmental Science

ORIGINAL RESEARCH
published: 08 February 2022
doi: 10.3389/fenvs.2021.793527

Prediction and Verification of Epimedium Flavonoids With Different Glycosylation Numbers in Reversing Glucocorticoid-Induced Bone Formation Inhibition by Molecular Docking and Zebrafish

Jun Jiang[1,2*†], *Jianpeng Xiao*[1†], *Jinjin He*[1], *Zhihui Cai*[1], *Jianping Chen*[2] *and Jiangning Yin*[3*]

[1]School of Pharmacy, Jiangsu University, Zhenjiang, China, [2]School of Chinese Medicine, the University of Hong Kong, Hong Kong, Hong Kong, China, [3]Emergency Department, the Affiliated Jiangning Hospital of Nanjing Medical University, Nanjing, China

Glucocorticoids have been detected in environmental waters, and their biological potency has raised concerns on their impact on aquatic vertebrates especially fish. Numerous researches showed that the continuous and direct contact of aquatic vertebrates with glucocorticoid contaminants in environmental water will cause bone formation inhibition. The aim of this study is to predict and verify the effect of icaritin (IT), icariin (ICA), and baohuside-I (BHG-I) in reversing glucocorticoid-induced bone formation inhibition (GIBFI) by molecular docking and zebrafish model. We contrasted their activity in reversing GIBFI from their affinity to bone metabolism proteins (OPG, RANKL, BMP-2, BMP-4, Runx-2) by molecular docking. Subsequently, zebrafish model was adopted to evaluate their reverse effects on GIBFI. Alizarin red staining coupled with image quantification were performed to evaluate the effects of ICA, IT, and BHG-I on skeleton stained area (SSA) and cumulative optical density (COD). Inductively coupled plasma-mass spectrometry was applied to determine the contents of bone mineral elements (CBME, Mg, K, Ca, Fe, Zn) in zebrafish bones. Docking results showed the receptors (BMP-2, BMP-4, and Runx2) all combined well to ICA, while BHG-I bound well to OPG, the affinity between IT and the above targets were the weakest. Fortunately, IT, ICA, and BHG-I significantly increased the SSA, COD, and the contents of Ca compared with the model group ($p < 0.05$) in the order of IT>ICA>BHG-I. In conclusion, the glycosyl groups increased the H-bond affinity between flavonoids and target sites, which weakened bone formation. IT, BHG-I, and ICA all alleviated GIBFI, but their intensity order was IT>ICA>BHG-I.

Keywords: glucocorticoid, zebrafish, bone formation inhibition, icaritin, icariin, baohuside-I, molecular docking

OPEN ACCESS

Edited by:
Hai Ocean Xu,
Jiangsu University, China

Reviewed by:
Shuying Li,
Zhejiang University, China
Wenhui Qiu,
Southern University of Science and Technology, China

***Correspondence:**
Jun Jiang
jiangjuntcm2007@hotmail.com
Jiangning Yin
jsyinjn@163.com

†These authors have contributed equally to this work

Specialty section:
This article was submitted to Toxicology, Pollution and the Environment, a section of the journal Frontiers in Environmental Science

Received: *12 October 2021*
Accepted: *14 December 2021*
Published: *08 February 2022*

Citation:
Jiang J, Xiao J, He J, Cai Z, Chen J and Yin J (2022) Prediction and Verification of Epimedium Flavonoids With Different Glycosylation Numbers in Reversing Glucocorticoid-Induced Bone Formation Inhibition by Molecular Docking and Zebrafish. Front. Environ. Sci. 9:793527. doi: 10.3389/fenvs.2021.793527

INTRODUCTION

Glucocorticoids are garnering research interests in recent years (Chen et al., 2017; Hidasi et al., 2017; Willi et al., 2018) as their potential environmental impacts are increasingly being recognized. They are frequently prescribed in medicine due to their anti-inflammatory, anti-allergic, and immunosuppressive properties (Willi et al., 2019). These compounds that originate from a wide range of medical applications in humans and domestic animals may pose an ecotoxicological risk for aquatic organisms in contaminated waters (McNeil et al., 2016; Neale et al., 2020).

The main source of these compounds entering the aquatic environment is the excretion of pharmaceutical residues used by either humans or animals in their free or conjugate forms (Goh et al., 2016). Existing treatment processes in wastewater treatment plants (WWTPs) are not entirely effective in removing these contaminants (Pedrouzo et al., 2009; Zwart et al., 2020). This can lead to pollutants transferring to the rivers and oceans *via* effluent of WWTPs (Cavallin et al., 2021). A previous study reported that total glucocorticoid levels had been detected at >0.5–52 ng/L in receiving river waters and up to 390 ng/L at discharged sites in Beijing region, China. Glucocorticoids and their metabolites totaling about 47–96 ng/L have been reported in Swiss river waters. In France, pharmaceutical industrial waste effluent detected with dexamethasone and prednisone up to 23,000 and 300 ng/L, respectively, have been discharged into a river where its downstream water was sampled over multiple time-points and estimated to contain 1–2,900 ng/L of dexamethasone and 50–1,260 ng/L of 6 α-methylprednisolone (Chen et al., 2017).

The continuous and direct contact of aquatic vertebrates with glucocorticoid contaminants in environmental water is a valid concern especially for fish (Leusch et al., 2017; Allijn et al., 2018). It has been shown that fishes that have long term exposure to hydrocortisone experience adverse effects in their locomotion, impeding aggressive behavior, a change in their immune response and possible modifications to their sexual behavior (Øverli et al., 2002; DiBattista et al., 2005). Also, it is demonstrated that in embryos, the glucocorticoid system is active after around 48 h post fertilization (Wilson et al., 2013). As it plays an important role in regulating hatching (Nesan et al., 2012), swimming activity (Castillo-Ramírez et al., 2019), circadian rhythm (Zhao et al., 2018), musculoskeletal development, growth and stress response (Apaydin et al., 2020), and exposure to exogenous glucocorticoids can be especially disruptive during early development. Relevant research reported prednisone induced decreased bone mineral density and bone loss (Schmid et al., 2020a; Schmid et al., 2020b). Furthermore, the long-term use of glucocorticoids will induce osteoporosis mediated by glucocorticoid receptor-dependent and -independent pathways (Zhao et al., 2016; Zhao et al., 2018). In our present study, we focused on the effects of glucocorticoids in aquatic environment on zebrafish bone formation and tried to find therapeutic drugs from traditional Chinese medicine.

Epimedii Folium (EF) has been used to repair fractures, bone and joint damage, and gonad dysfunctions for thousands of years (Zhang et al., 2018). The major active flavonoids in EF were icariin (ICA), baohuside-I (BHG-I), BHG-II, and epimedin (A, B, C) (Li et al., 2015). There is little Icaritin (IT) in Epimedium herbs and extractions, while EF-flavonoids can be biologically converted into IT *in vivo* after hydrolysis of glycosidic bonds. IT was the structural parent nucleus of ICA and BHG-I, and the glycosylation number of IT, BHG-I, and ICA were 0, 1, 2, respectively (**Figure 1**). Previous studies revealed that higher concentrations of IT were discovered in rat plasma, urine, and feces after oral administration of ICA or BHG-I (Sun et al., 2014; Sun et al., 2016). Pharmacological studies confirmed that ICA increased bone mass and prevent glucocorticoid-induced apoptosis in osteocytes (Feng et al., 2013; Wang et al., 2018). In addition, BHG-I activated EGFR-Akt-Nrf2 signaling and protected osteoblasts from Dexamethasone (Liu et al., 2017). Also, relevant studies have reported that IT exerted positive effects on human osteoblast proliferation and osteogenic function (Lim et al., 2017). Up to now, there are barely documents reported the activity difference of IT, BHG-I, and ICA in anti-bone formation inhibition.

The skeletons were in constant renewal, and this steady state of bone was mainly maintained by osteoclasts and osteoblasts. Considerable evidence indicated that the osteoprotegerin (OPG)/receptor activator of nuclear factor κB ligand (RANKL)/RANK system (OPG/RANKL/RANK) was relevant to osteoclast proliferation and differentiation (Liu and Zhang, 2015; Kushlinskii et al., 2017). Bone morphogenic protein (BMP), a member of the transforming growth factor-beta (TGF-b) super family (Aslani et al., 2019), was related to the differentiation of osteoblasts from mesenchymal stem cells or osteoprogenitor cells in bone marrow (Garg et al., 2017; Liu L. et al., 2018; Yang et al., 2018). It was demonstrated that pharmacologic blockade of RANKL in the OPG/RANKL/RANK system was an effective treatment for osteoporosis. Similarly, antagonists, such as noggin (Hashimi, 2019), chordin (Tekari et al., 2017), and gremlin-1, also effectively restricted the differentiation of osteoblasts through binding to BMP-2 (Kišonaitė et al., 2016). All these results demonstrated that binding to bone metabolism-related protein targets was one important way for drugs to promote or inhibit bone turnover. The structural difference in the glycosyl groups of IT, BHG-I, and IT caused their discrepancy in affinity with related targets, which was one significant factor for their bioactivity in anti-bone formation inhibition.

In this paper, we primarily contrasted the activity difference of IT, BHG-I, and ICA on anti-bone formation inhibition and clarified the underlying mechanism. Molecular docking was carried out to elaborate the affinity between three flavonoid homologs (IT, BHG-I, and ICA) and protein targets. Immediately, the zebrafish models were used to verify the molecular docking results and evaluates their effects in anti-bone formation inhibition according to skeleton staining, quantification of the area of mineralized bones and cumulative optical density, and determination of bone mineral contents. Finally, the order of action intensity of these three flavonoids in anti-bone formation inhibition was obtained, and the mechanism of this difference was explained from the perspective of the interaction between chemical structure and bone metabolic protein targets.

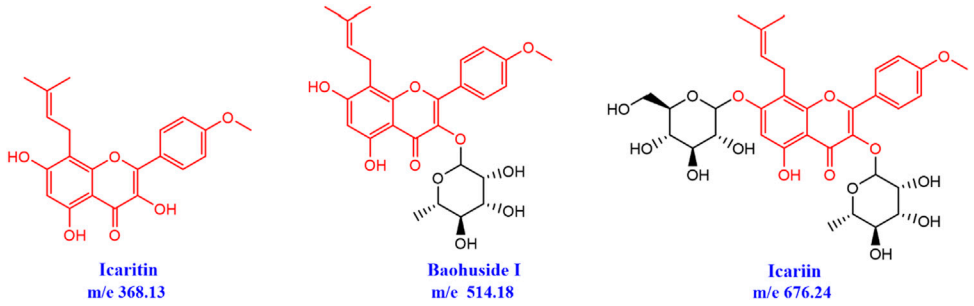

FIGURE 1 | Chemical structures of icaritin (IT), baohuside-I (BHG-I), and icariin (ICA).

MATERIALS AND METHODS

Molecular Docking Simulation

The amino acid sequences of OPG (PDB ID: 3URF, CHAIN: Z, Length: 171 AA, Residues: 22–186), RANKL (PDB ID: 3URF CHAIN: A Length: 162 AA Residues: 162-317) and BMP-2 (PDB ID: 2QJB CHAIN: AB Length: 116 AA Residues 283–396) have structural data of Experimental Analytical proteins. BMP-4 and Runx2 amino acid sequences have no experimental analytical protein structure data, and 3D protein structure data was obtained by homology modeling. Data were calculated using Molecular Operating Environment 2015.10 software (Chemical Computing Group Inc., Quebec, Canada). Maestro was carried out to build the structure of ligands, and then they were transformed into 3D format. The docking module was used to dock the ligand, and the protein and docking scores were evaluated by Glide's scoring function.

Animals

Zebrafish farming was conducted according to the standard procedure (Varga et al., 2018). Adult zebrafish mate and spawn naturally under the condition of 10/14 h dark/light cycle. The zebrafish embryos and larvae were cultured in six-hole plates with blank E_3 medium solution (5.0 mM NaCl, 0.17 mM KCl, 0.33 mM $CaCl_2$, and 0.33 mM $MgSO_4$) in Light incubator (PGX-150B) at 28.5°C and natural air circulation. Animal experiments were carried out in accordance with the Guidelines for Animal Experimentation of Jiangsu University (Zhenjiang, China), and the protocol was approved by the Animal Ethics Committee of this institution.

Treatment Regime

The zebrafish model by prednisolone (PNSL, 25 μM) was established according to our preliminary study (Jiang et al., 2018). Zebrafish larvae were randomly divided into seven groups ($n = 15$ larvae in each well with three replications) as follows: Control (CK, blank E_3 medium), DMSO (DMSO, 0.5% DMSO), Model group (MX, 25 μM PNSL), Disodium ethydronate (YTLSN, 15 μM Disodium ethydronate + 25 μM PNSL), Icaritin (IT, 0.1, 1.0, or 10.0 μM IT + 25 μM PNSL), Baohuside-I (BHG-I, 0.1, 1.0, or 10.0 μM BHG-I + 25 μM PNSL), and Icariin (ICA, 0.1, 1.0, or 10.0 μM ICA + 25 μM PNSL) 3 days after fertilization (DAF). From 6 to 10 DAF, larvae were fed with paramecia for 1 h every day. Following each feeding, the remaining paramecia were washed out, and the medium was replaced with blank E_3 medium-containing drugs or not (Jiang et al., 2018).

Behavior Analysis

After 4 days of drug deliveries, zebrafish locomotor activity was monitored by EthoVision behavior system. Prior to the start of tracking, the software needed to be calibrated. The video sampling rate was 25 frames per second (fps), based on the design recommendations (Wolter and Svoboda, 2020). First, under the "Trial List," one trial was selected. For the "Arena Settings," each well/arena was calibrated based on the diameter of the well. The diameter of the wells within the well plates used in this manuscript are 96 well plate (6.54 mm). For the "Detection Settings," dynamic subtraction was selected and the dark contrast and subject contour were adjusted to optimize tracking efficiency (Knafo and Wyart, 2018). Within the "Analysis Profiles," the selected dependent variables were distance moved, velocity, and time spent moving. These endpoints were based on the center-point activity of the larvae (Martella et al., 2016). The results were then exported to Excel and statistical analysis software suites. According to the methods described above, moving distance (MD), average speed (AS), travel frequency (TF), and hotspot are selected as the anti-GIBFI drug efficiency evaluation index in this model.

Whole-Mount Skeletal Staining

Alizarin red staining on zebrafish larvae was performed as previously described (Bruneel et al., 2015). Briefly, the zebrafish larvae were collected at 10 DAF, all the zebrafish were killed by 3-aminobenzoic acid ethyl ester methane sulfonate (MS-222, 100 mg/L) (Martini et al., 2021). After removal of MS-222 solution, zebrafish larvae were fixed in paraformaldehyde solution 4% in PBS (pH 7.4) and stained with Alizarin red staining (Vimalraj et al., 2020). Fresh prepared bleach with 1.5% H_2O_2 and 1% KOH was added 12 h later after the staining solution was removed and washed., All samples were decolored with glycerol 1 h later, and the stained zebrafish was placed under a microscope to observe their stained bones (Lim et al., 2021). Images were acquired by microscope (Olympus IX71/IX81, Olympus Corporation, Japan). Digital images were analyzed using

TABLE 1 | Regression equations, correlation coefficient, linear range, and LLOD of ICP-MS detection.

Element	Regression equation	r^2	Linear range (μg/L)	LLOQ (μg)
Mg	Y = 3,086.1369X + 1,838.2667	0.9999	0.1–10.0	0.5
K	Y = 7,150.6463X + 183,107.5167	0.9999	0.01–10.0	0.5
Ca	Y = 7.6893X + 242.9667	0.9999	0.5–50.0	0.5
Fe	Y = 24,740.9960X + 28,669.6067	0.9999	0.01–10.0	0.5
Zn	Y = 5,916.4495X + 2,140.5267	0.9999	0.001–10.0	0.5

Note. ICP-MS, inductively coupled plasma-mass spectrometry; LLOQ, lower limit of quantitation.

ImageJ software (National Institutes of Health, Bethesda, MD, USA) to quantify the skeleton stained area (SSA) and cumulative optical density (COD) ($n = 15$) (Cheng et al., 2017; Liu S. et al., 2018).

Sample and Standard Solution Preparation for Inductively Coupled Plasma-Mass Spectrometry Detection

The mineral contents in zebrafish larvae were measured by inductively coupled plasma-mass spectrometry (ICP-MS) as reported in our previous study. The larvae were collected at 10 DAF ($n = 15$) and washed five times in double distilled water and then transferred to centrifuge tubes. Immediately, samples were digested with 70% HNO_3 in a microwave oven for 4 h. Determination of Ca, K, Mg, Zn, and Fe was carried out by the 7500cx ICP/MS system (Agilent Technologies, Santa Clara, CA, USA) equipped with a G3160B I-AS integrated autosampler.

The standard solutions of Mg, K, Ca, Fe, and Zn with mass concentration at 10 mg/L were diluted into tuning solution (1 μg/L) with 2% nitric acid. The series concentration of Ca standard solution was 0, 40, 80, 120, 160, 200 mg/L. The other series concentration of Mg, K, Zn, and Fe standard solution were 0, 10, 20, 40, 80, 160 μg/L.

Inductively Coupled Plasma-Mass Spectrometry Conditions

Agilent 7500 ICP-MS system was used for simultaneous determination of Ca, K, Mg, Zn, and Fe. The pressure of Ar and He were set to 700 and 40 KPa, respectively. Circulating water temperature was 20°C. The pressure was 230–400 KPa. The exhaust air volume was set to 5,000–7,000 L/min. Plasma power was 1.5 KW. Carrier gas flow rate was 0.9 L/min, and compensation gas flow rate was 0.25 L/min. Injection depth was 8 mm. Peristaltic pump speed was set to 0.1 r/s. Premix chamber temperature was 2°C.

Method Validation of Inductively Coupled Plasma-Mass Spectrometry

After the instrument was tuned, the series mixed standard working solution was injected into ICP-MS, and the signal response value of each element was measured. The mass concentration was taken as the abscissa, and the response signal value was taken as the ordinate. The correlation coefficient (r) of the standard curve were all higher than 0.9990. The detailed calibration curves, linear range, and the lower limit of quantitation (LLOQ) for mineralized elements are available in **Table 1**.

Statistical Analysis

All data were presented as the mean ± SD. Statistical analysis was performed using GraphPad Prism 5 (GraphPad software, USA). Differences were analyzed by one-way analysis of variance (Tukey, compare all pairs of columns). Differences with $p < 0.05$ were considered significant.

RESULTS

Molecular Docking Results

The important parameters obtained from molecular docking included docking scores, interacting residues, bonding energy, binding position and H-bonds interaction between receptors and ligands. The ICA-RANKL interaction had 4 H-bond residues as GLU292 (A), ASP174 (A), SER252 (A), and LYS205 (A) with a total binding energy of −12.8 kcal/mol. The interaction between BMP-2 and ICA also had 4 H-bond residues as GLU46 (A), GLY45 (A), CYS47 (A), and CYS79 (A) with a total binding energy of −11.5 kcal/mol. ICA bound to BMP-4 *via* H-bond interaction at LEU 386(B), pi-H interactions with TRP 325(B), and TRP 322(B) with a total binding energy of −3.6 kcal/mol. The ICA-RANK interacted at GLN122, LEU143, and GLN144 with a total binding energy of −3.7 kcal/mol. Therefore, the docking results indicated that ICA could bind to multiple protein targets including RANKL, BMP-2, BMP-4, RANK, and Runx2 with docking scores at −6.67224169, −6.69499111, −6.68158722, −6.81634808, and −6.87304401, respectively (**Tables 2** and **3**; **Figure 2**, **Supplementary Figure S1**).

Although BHG-I could interact with the above six protein targets, the combination between BHG-I and OPG *via* pi-H interactions with interacting residues TYR 71(Z) and VAL 72(Z), H-bond interaction with LYS 87(Z) had the maximum absolute docking score (−9.64769459, **Table 2**) and the lowest binding free energy (−3.5 kcal/mol, **Table 3**). Similarly, ligand IT was able to communicate with OPG, BMP-2/-4, and RANK, but their absolute docking score were relatively smaller than ICA and BHG-I, which showed that the combination of IT and the above targets were weak. The IT-OPG interaction had two residues as TYR71, VAL65 with a total binding energy of −1.5 kcal/mol. The IT connected with BMP-2 through GLU109 residues with a

TABLE 2 | Docking scores and interacting residues between receptors and ligands.

Receptor	Ligand	S	Residues
OPG	Icariin	−8.56518173	TYR71, VAL72, LYS87
	Baohuside I	−9.64769459	
	Icaritin	−8.96370506	TYR71, VAL65
RANKL	Icariin	−6.67224169	LYS205, GLU292, SER252, ASP174
	Baohuside I	−6.09861946	ASP230, LA232, ASN295
	Icaritin	−5.79909897	
BMP-2	Icariin	−6.69499111	LYS47, GLY45, GLU46, CYS79
	Baohuside I	−5.87657118	ARG16, GLU109
	Icaritin	−5.29828167	GLU109
RANK	Icariin	−6.68158722	GLN122, LEU143, GLN144
	Baohuside I	−6.76106215	CYS112, ARG111, ASP93
	Icaritin	−5.86958647	VAL91, CYS92
BMP-4	Icariin	−6.81634808	LEU386, TRP325, TRP322
	Baohuside I	−6.19196224	GLU388
	Icaritin	−5.70623016	GLU388, TRP325, TRP322, TYR385
Runx2	Icariin	−6.87304401	LEU168
	Baohuside I	−5.74639988	HIS214, ARG115
	Icaritin	−5.46986055	

Note. OPG, osteoprotegerin.

binding energy of −1.1 kcal/mol. The IT-RANK interaction had two residues as VAL91 and CYS92 with a total binding energy of −1.8 kcal/mol. The IT-BMP-4 interaction had four residues as GLU388, TRP325, TRP322, and TYR385 with a total binding energy of −7.3 kcal/mol. The IT connected with Runx2 through LEU168(A) residues with a binding energy of −5.7 kcal/mol. These results exhibited that the affinity between BHG-I and OPG was the strongest, and the combination of IT and above targets were all instability.

Effect of Icariin, Icaritin, and Baohuside-I on Bone Formation and Bone Mineralization

The skeleton stained area (SSA) and cumulative optical density (COD) were important indicators of bone mineralization. Alizarin Red staining was widely used to detect and quantify mineralized bones because it was capable of binding to calcium salts and showed red under the microscope (**Figure 3**). Compared with the DMSO group, the area of SSA and COD in Zebrafish larvae were decreased significantly under the treatment of 25 μM PNSL (MX, $p < 0.01$, **Figure 4**). These results indicated that PNSL reduced bone mineralization and inhibited osteogenic differentiation in zebrafish larvae. Compared with the MX group, the COD was significantly increased ($p < 0.05$, **Figure 4A**) under the intervention of IT (0.1, 1.0, and 10.0 μM), BHG-I (10.0 μM), and ICA (0.1, 1.0, and 10.0 μM). Furthermore, compared with the MX group, the SSA in ICA, IT, and BHG-I all showed significant increase from 0.1 to 10.0 μM ($p < 0.05$, **Figure 4B**). These flavonoids showed a prospective concentration-dependent in reversing PNSL induced inhibition of bone formation.

Effect of Icariin, Icaritin and Baohuside on Zebrafish Behavior

The behavior analyzer—Ethovision—was used to track the movement of zebrafish. As shown in **Figures 5** and **6**, the moving speed (MS), moving distance (MD), and travel frequency (TF) of PNSL group was significantly lower than those of the DMSO, while for YTLSN and all three compounds, these parameters were close to the control. The results showed that different concentrations of IT, ICA, and BHG-I increased MD by 131.50%, 124.66%, and 107.38%, respectively, with partial significant (p-value < 0.001–0.01). TF for IT, ICA, and BHG-I were 169.39%, 137.66%, and 128.57%, respectively. Also, the hot plot revealed zebrafish activity degree (**Supplementary Figure S2**). These results with significant differences demonstrated that IT, ICA, and BHG-I could reverse GIBFI.

Icariin, Icaritin, and Baohuside Promote the Enrichment of the Elements Required for Bone Mineralization

Bone was composed of 69–80 wt% calcium phosphate and other trace elements. To confirm the therapeutic effect of ICA, IT, and BHG-I on osteogenesis, whole-body Ca, K, Mg, Zn, and Fe contents of larvae were measured by ICP-MS. Compared with the DMSO, the treatment of PNSL significantly decreased whole-body Ca, K, Mg, Zn, and Fe levels by 6.24, 1.67, 1.06, 0.11, and 0.75, respectively ($p < 0.05$). After the treatment of IT, ICA, and BHG-I, whole-body Ca, K, Mg, Zn, and Fe levels were significantly higher than PNSL group ($p < 0.05$, **Supplementary Figure S3**, **Figures 5**).

DISCUSSION

The OPG/RANKL/RANK signaling pathway plays a crucial role in regulating the bone remodeling process (Khosla, 2001). RANKL binds to RANK on osteoclasts to stimulate differentiation. OPG can also bind to RANKL to block this process and to control the remodeling process (Tyrovola,

TABLE 3 | Bonding energy, binding position, H-bond interaction between receptors and ligands.

Receptor	Ligand	Position	Receptor	Interaction	Distance(Å)	E (kcal/mol)
OPG	Icaritin	O (5)	TYR 71(Z)	H-acceptor	2.89	−0.9
		6-ring	VAL65(Z)	pi-H	4.37	−0.6
	Baohuside I	O (7)	LYS 87(Z)	H-acceptor	3.62	−1
		6-ring	TYR 71(Z)	pi-H	3.79	−0.8
		6-ring	VAL 72(Z)	pi-H	4.32	−1.7
RANKL	Icariin	O (6)	GLU292(A)	H-donor	2.86	−1.8
		O (9)	ASP174(A)	H-donor	2.96	−2.9
		O (6)	SER252(A)	H-acceptor	2.85	−1.5
		O (11)	LYS205(A)	H-acceptor	2.94	−6.6
	Baohuside I	O (4)	ASN 295(A)	H-donor	3.23	−1.2
		O (8)	ASP 230(A)	H-donor	2.82	−3.6
		O (7)	ALA 232(A)	H-acceptor	3.17	−1.7
BMP-2	Icariin	O (6)	GLU46 (A)	H-donor	2.9	−3.8
		O (7)	GLY45 (A)	H-donor	2.88	−2.5
		O (7)	CYS47(A)	H-donor	3.43	−1.3
		O (13)	CYS79 (A)	H-donor	2.9	−3.9
	Baohuside I	O (8)	GLU109 (A)	H-donor	2.86	−3.3
		6-ring	ARG16 (A)	pi-H	4.18	−4.7
	Icaritin	O (3)	GLU 109 (A)	H-donor	2.86	−1.1
RANK	Icariin	O (9)	GLN122(A)	H-donor	3.02	−0.9
		O (11)	LEU143(A)	H-donor	3.15	−0.7
		O (13)	GLN144(A)	H-donor	3.15	−2.1
	Baohuside I	O (7)	CYS112 (A)	H-donor	3.4	−0.4
		O (3)	ASP93 (A)	H-acceptor	3.24	−1.2
		6-ring	ARG111 (A)	pi-H	4.05	−0.9
	Icaritin	O (2)	VAL91 (A)	H-donor	2.95	−1.1
		6-ring	CYS92(A)	pi-H	4.59	−0.7
BMP-4	Icariin	O (10)	LEU386(B)	H-donor	3.23	−0.9
		C (24)	TRP325(B)	H-pi	3.59	−0.6
		O (13)	TRP322(B)	H-pi	3.58	−2.1
	Baohuside I	O (9)	GLU388(B)	H-donor	2.96	−4.1
	Icaritin	O (2)	GLU388(B)	H-donor	2.98	−5.3
		C (25)	TRP325(B)	H-pi	3.7	−0.6
		C (27)	TRP322(B)	H-pi	3.94	−1.4
		6-ring	TYR385(B)	H-pi	3.74	0
Runx2	Baohuside I	O (9)	HIS214(A)	H-donor	3	−1.7
		O (3)	ARG115(A)	H-acceptor	3.1	−2.5
	Icaritin	O (4)	LEU168(A)	H-donor	2.74	−4.4
		6-ring	LEU168(A)	pi-H	3.84	−1.3

2015; Kovács et al., 2019; Li et al., 2019). If ligands bound to OPG, blocking the binding of OPG to RANKL, which weakened the inhibitory effect of ligand to osteoclasts. On the other hand, if the ligands combined with RANKL which also inhibited the interaction of RANKL-RANK and attenuated the differentiation of osteoclasts, and finally showed bone resorption inhibition (Jiang et al., 2018). Antagonists, such as noggin (Chien et al., 2020), chordin (Huang et al., 2019) and gremlin-1 (Silvério de Barros et al., 2019), effectively restrict osteoblast differentiation through binding to BMP-2. Similarly, the combination between ligand and Runx2 blocked the function of Runx2 in promoting osteogenic differentiation. In summary, the ligands bind to BMP-2, BMP-4, or Runx2 inhibited the differentiation of osteoblasts, the stronger the binding, the more inhibition on the bone formation.

In molecular docking, the lower bonding energy, the more stable binding between the ligands and the receptors. In addition, the larger the absolute value of docking scores, the more stable the combination. From the docking scores, the binding between BHG-I and OPG (−9.64769459) was the most stable compared with that of IT (−8.96370506) and ICA (**Table 2**). Meanwhile, the interaction between BHG-I and OPG had the lowest binding energy (−3.5 kcal/mol, **Table 3**, **Figure 2**). According to the docking results, the position of H-bonds was mostly located in glycosylation, which indicated that glycosylation affected the formation of H-bonds. For example, BHG-I bound to OPG *via* pi-H interactions with interacting residues TYR 71(Z), and VAL 72(Z), H-bond interaction with LYS 87(Z), while IT bound to OPG was pi-H interaction at VAL 65(Z) and H-bond interaction at TYR 71(Z). The glycosyl groups in BHG-I promoted the formation of H-bond and the interaction of ligand-receptor, which ultimately manifested as the weakening of anti-GIBFI. The formation of more H-bonds between ICA and multiple bone turnover targets was mainly attributed to the two glycosyl groups in its structure. Therefore, the binding between ICA and above protein targets was easier and more stable than the other two flavonoids because of the less glycosyl groups in IT and BHG-I (0 and 1, respectively). Based on molecular docking, the

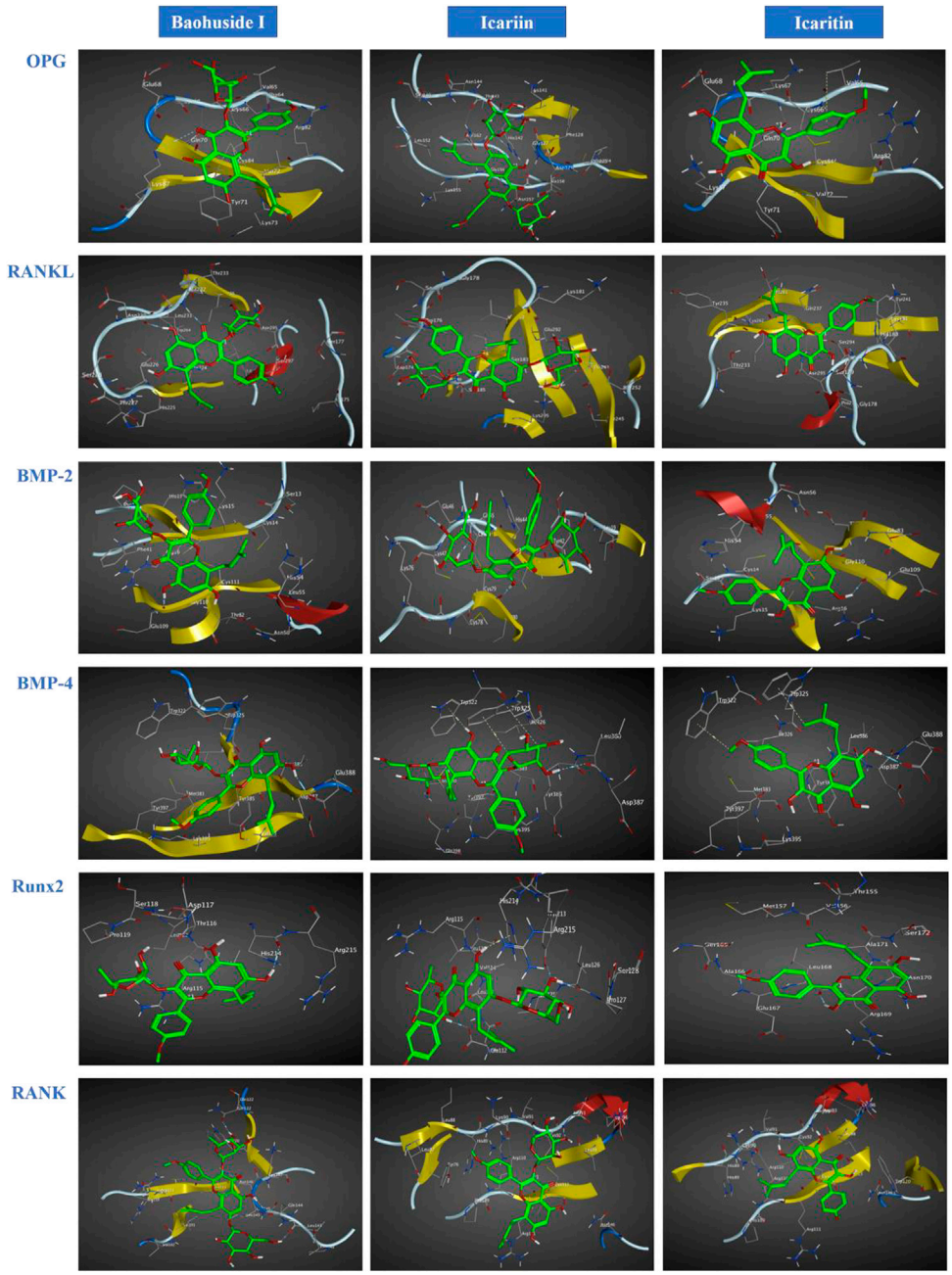

FIGURE 2 | Optimal interaction of the receptors with small molecule ligands. Receptors: OPG, RANKL, RANK, BMP-2, BMP-4, and RUNX-2; Ligands: BHG-I, ICA, IT.

receptors (RANKL, BMP-2, BMP-4, and Runx2) all combined well to ICA, while BHG-I bound well to OPG, the combination of IT and the above targets was the weakest. It was predicted that the anti-GIBFI effect of IT was stronger than that of ICA and BHG-I.

Zebrafish was an ideal animal model *in vivo* for studying bone deformations for its high skeletal and genetics similarity to human skeleton (Luo et al., 2016; Zhao et al., 2020). The zebrafish larvae contained the sufficient and necessary cells for both bone formation and resorption activity (Luo et al., 2016). Alizarin red staining is a special stain used for bone staining. This stain can be used to determine the bone mineralization level based on the color, and the area of alizarin red staining can be used to determine efficacy of drugs affecting bone mineralization. The indicators observed in this study were the COD and SSA value, which directly reflects the differentiation and number of osteoblasts. Osteoblast differentiation and bone formation can be visualized in the zebrafish larvae by monitoring the changes of dyeing area.

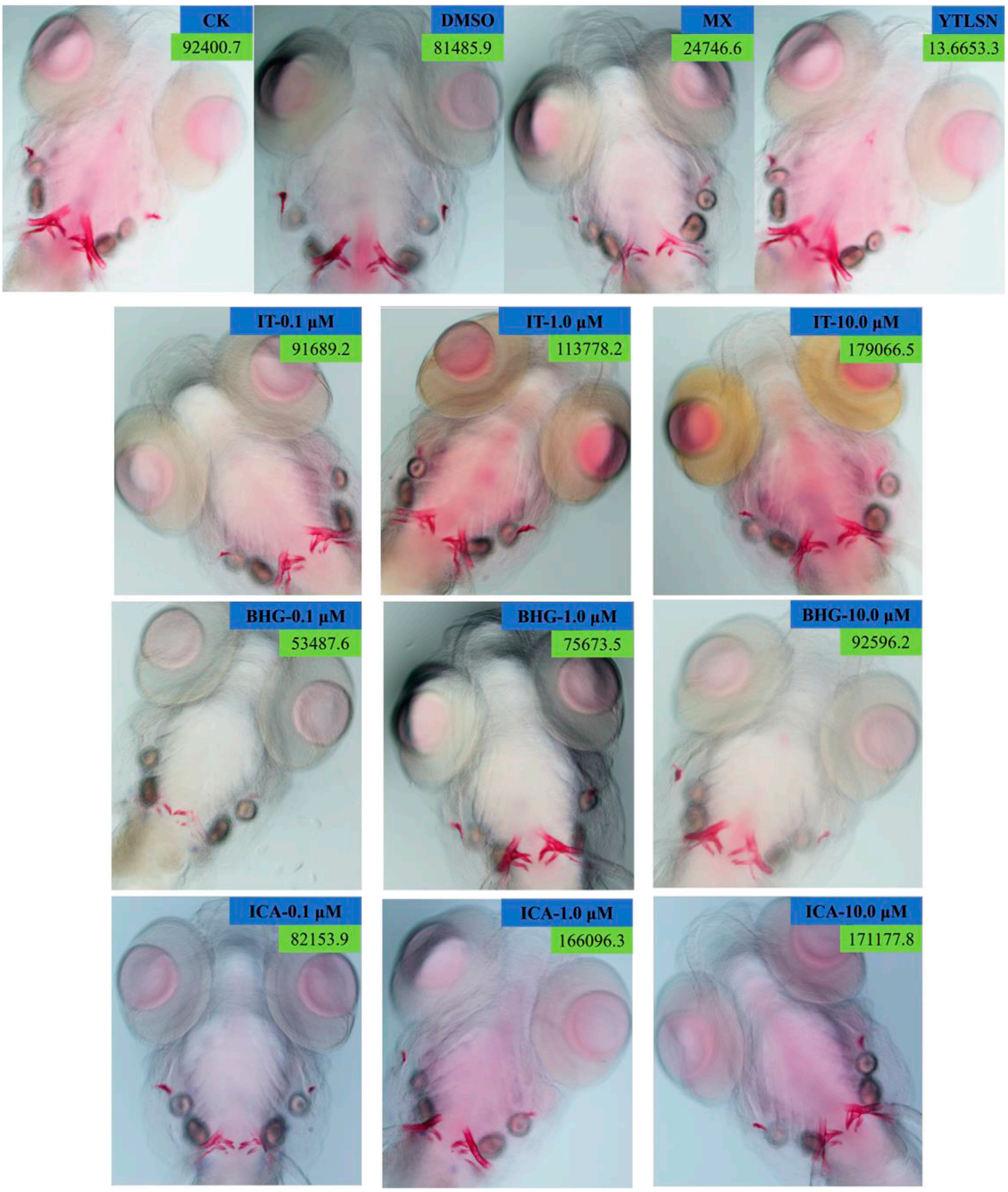

FIGURE 3 | Ventral view of Alizarin Red stained zebrafish skull at 10 DAF (×100). CK, blank E_3 medium; DMSO, 0.5% DMSO; MX, 25 μM PNSL; YTLSN, 15 μM disodium ethydronate + 25 μM PNSL; ICA, 0.1, 1.0, or 10.0 μM ICA + 25 μM PNSL; BHG-I, 0.1, 1.0, or 10.0 μM BHG-I + 25 μM PNSL; IT, 0.1, 1.0, or 10.0 μM IT + 25 μM PNSL.

Our results indicated that PNSL exposure significantly inhibited osteogenic differentiation and bone mineralization in zebrafish larvae ($p < 0.05$, **Figure 4**). After the drug intervention, IT, ICA, and BHG-I all exerted positive effects on reversing PNSL-induced osteopenia in zebrafish ($p < 0.05$). According to the COD and SSA results, the reversal effect of IT and ICA on bone formation inhibition reached or even exceeded that of positive drugs, especially at 10 μM (**Figure 4**). This phenomenon was reproduced in the results of bone mineral element contents. As shown in **Table 4** and **Supplementary Figure S3**, the levels of Mg, K, Ca, Fe, and Zn were achieved or even exceeded that of YTLSN group. BHG-I was weaker than IT and ICA in increasing SSA, COD, and bone mineralized elements.

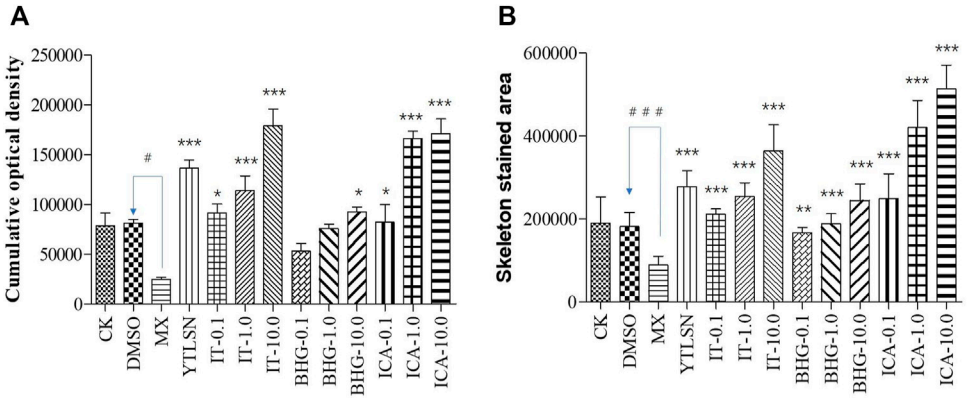

FIGURE 4 | The effect of ICA, IT, and BHG-I- I on mineralization in zebrafish larvae (n = 15). **(A)** Calculation of cumulative optical density. **(B)** Calculation of mineralized area. CK, blank E3 medium; DMSO, 0.5% DMSO; MX, 25 μM PNSL; YTLSN, 15 μM disodium ethydronate + 25 μM PNSL; ICA, 0.1, 1.0 or 10.0 μM ICA + 25 μM PNSL; BHG-I, 0.1, 1.0 or 10.0 μM BHG-I + 25 μM PNSL; IT, 0.1, 1.0 or 10.0 μM IT + 25 μM PNSL. #p < 0.05 compared with DMSO, ###p < 0.001 compared with DMSO, *p < 0.05 compared with MX. **p < 0.01 compared with MX, ***p < 0.001 compared with MX.

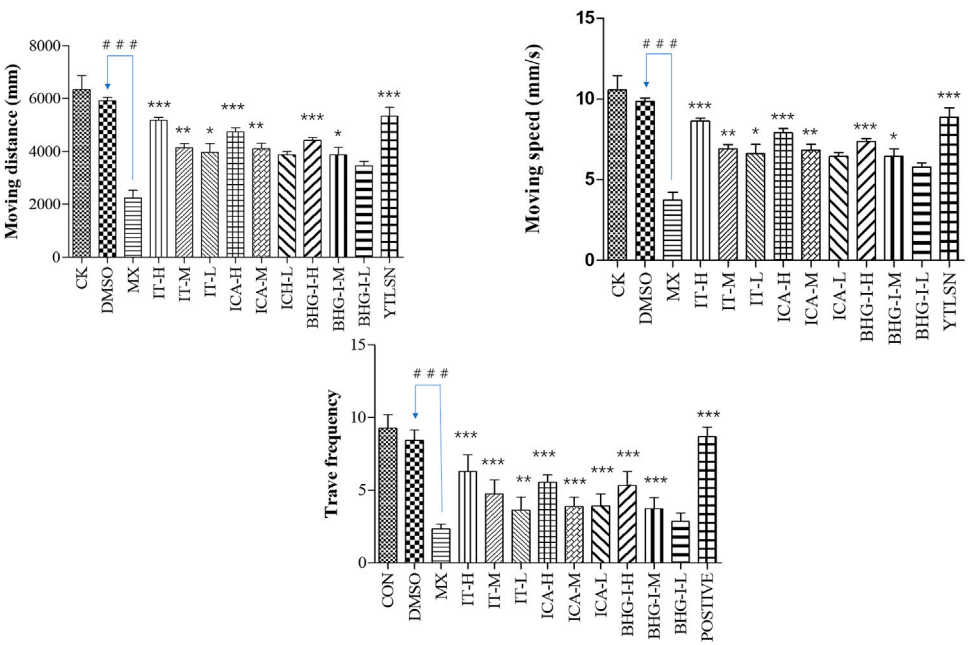

FIGURE 5 | Effect of ICA, IT, and BHG-I on behavioral analysis (n = 15). CK, blank E_3 medium; DMSO, 0.5% DMSO; MX, 25 μM PNSL; YTLSN, 15 μM disodium ethydronate + 25 μM PNSL; ICA, 0.1, 1.0 or 10.0 μM ICA + 25 μM PNSL; BHG-I, 0.1, 1.0, or 10.0 μM BHG-I + 25 μM PNSL; IT, 0.1, 1.0 or 10.0 μM IT + 25 μM PNSL. ###p < 0.001 compared with DMSO. *p < 0.05 compared with MX. **p < 0.01 compared with MX. ***p < 0.001 compared with MX.

Behavioral changes of zebrafish have been linked to chemical exposure (Pitt et al., 2018; Nunes et al., 2020). Behavior analyzer—Ethovision XT—made it possible to examine numerous motor events and facilitates quantitative analysis of behavior (Zheng et al., 2021). The behavioral change in zebrafish is an important indicator to evaluate the anti-GIBFI effect of ICA, IT, and BHG-I. The MD and TF in PNSL group further supported that the construction of osteoporosis model was successful. MDs for IT, ICA, and BHG-I were 60.32%–131.50%, 71.59%–112.10%, 47.63%–97.38%, respectively. These results with significant differences demonstrated that ICA, IT, and BHG-I could improve dyskinesia of zebrafish to some extent.

According to the above discussion, the docking results indicated the affinity difference was ICA>BHG-I>IT. The more stable the binding, the stronger the effect of inhibiting the formation of osteoblasts and the less the effect of anti-GIBFI. In consequence, the order of their intensity in reversing GIBFI should be IT>BHG-I>ICA. Theoretically, anti-GIBFI effect of BHG-I, a single-glucose-containing flavanone glycoside, should

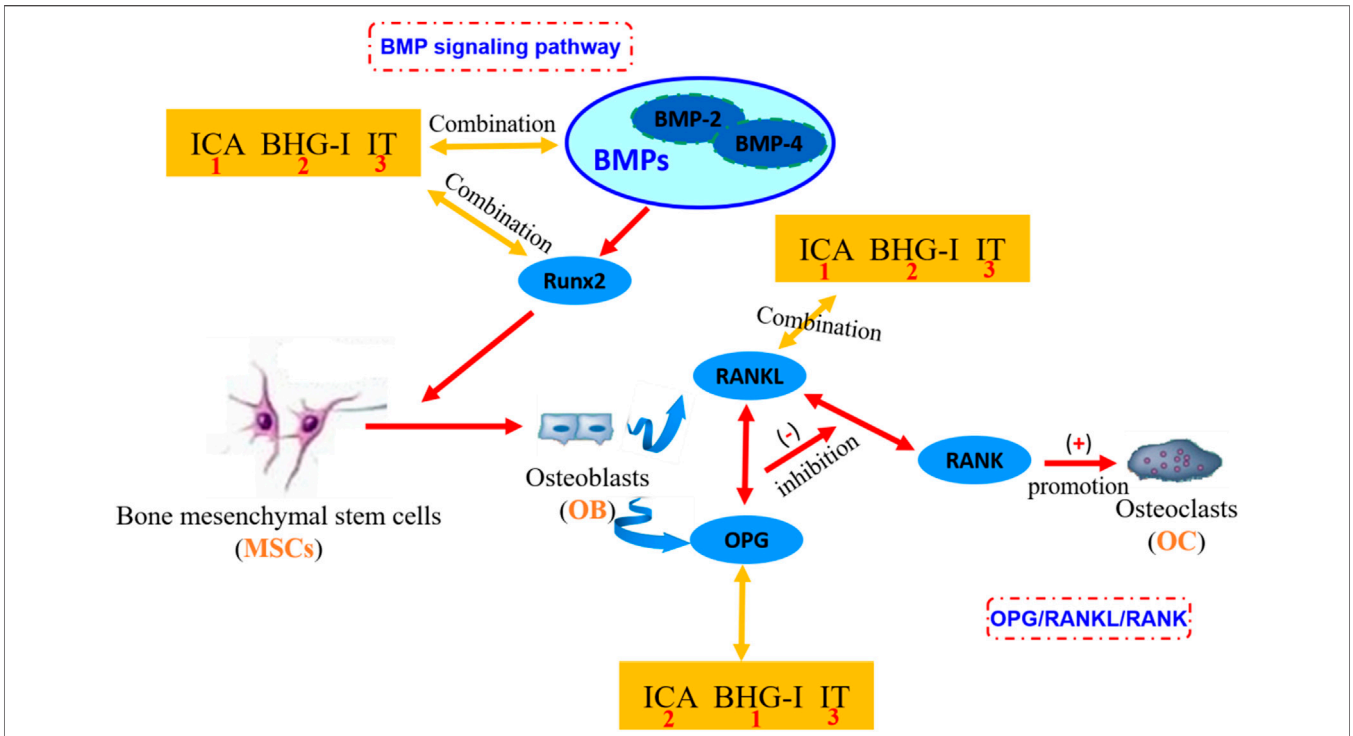

FIGURE 6 | The mechanism of affinity/bioactivity of EF-flavonoids and bone metabolism targets. ICA, icariin; BHG-I, baohuside I; IT, icaritin. In the figure, the orange square frames are in the symbol of the small molecule ligands ICA, BHG-I, and IT. The blue boxes represent the protein targets in OPG/RANKL/RANK system or BMP signaling pathway. The numbers in the orange square frames represent the affinity of the compound with bone metabolic protein targets. The number 1 represents the combination between compound and target is more stable. These three compounds are equivalent to antagonists of bone metabolic targets. The more stable the binding, the less the effect of anti-GIBFI. This graph clearly shows the combination between receptors and protein targets. EF, Epimedii Folium; GIBFI, glucocorticoid-induced bone formation inhibition.

TABLE 4 | Effect of ICA, IT, and BHG-I on the mineral contents in zebrafish larvae.

	Mg	K	Ca	Fe-56	Zn
CK	1.17 ± 0.054	1.80 ± 0.057	9.91 ± 1.29	0.82 ± 0.056	0.12 ± 0.013
DMSO	1.24 ± 0.083	1.76 ± 0.050	9.85 ± 1.32	0.83 ± 0.026	0.13 ± 0.020
MX	0.18 ± 0.069$^{###}$	0.089 ± 0.046$^{###}$	3.61 ± 0.99$^{###}$	0.084 ± 0.027$^{###}$	0.014 ± 0.0084$^{###}$
YTLSN	0.85 ± 0.028***	1.33 ± 0.10***	36.79 ± 2.60***	0.71 ± 0.086***	0.12 ± 0.0073***
BHG-0.1	0.28 ± 0.033	0.20 ± 0.033	15.62 ± 1.08***	0.058 ± 0.037	0.0094 ± 0.0062
BHG-1.0	0.39 ± 0.046	0.29 ± 0.076	18.88 ± 1.50***	0.18 ± 0.037	0.041 ± 0.0032
BHG-10.0	0.47 ± 0.047*	0.53 ± 0.044***	22.71 ± 1.64***	0.30 ± 0.088	0.053 ± 0.0062*
ICA-0.1	0.48 ± 0.075*	0.50 ± 0.074**	20.11 ± 1.00***	0.14 ± 0.053	0.018 ± 0.0035
ICA-1.0	0.80 ± 0.18***	1.12 ± 0.14***	25.99 ± 0.94***	0.28 ± 0.044	0.038 ± 0.0043
ICA-10.0	1.35 ± 0.049***	1.48 ± 0.12***	29.27 ± 1.67***	0.58 ± 0.12***	0.079 ± 0.0066***
IT-0.1	0.62 ± 0.077***	0.66 ± 0.036***	23.53 ± 0.80***	0.52 ± 0.076***	0.077 ± 0.011***
IT-1.0	1.21 ± 0.16***	1.38 ± 0.11***	30.69 ± 2.99***	0.76 ± 0.044***	0.11 ± 0.017***
IT-10.0	1.79 ± 0.067***	1.87 ± 0.16***	37.61 ± 2.33***	1.01 ± 0.16***	0.18 ± 0.025***

Note. CK, blank E_3 medium; DMSO, 0.5% DMSO; MX, 25 μM PNSL; YTLSN, 15 μM disodium ethydronate + 25 μM PNSL; ICA, 0.1, 1.0, or 10.0 + 25 μM PNSL; BHG-I, 0.1, 1.0, or 10.0 μM BHG-I + 25 μM PNSL; IT, 0.1, 1.0, or 10.0 μM IT + 25 μM PNSL. Data are shown as mean ± standard error. $^{###}$*p < 0.001 compared with DMSO.* **p < 0.05 compared with MX.* ***p < 0.01 compared with MX.* ****p < 0.001 compared with MX. ICA, icariin; IT, icaritin; BHG-I, baohuside-I.*

have been stronger than ICA (the order should be IT>BHG-I>ICA), but the zebrafish experimental results were contrary to this (IT>ICA>BHG-I). ICA exhibited a more powerful potency against GIBFI than BHG-I with AMB values of 513,950.2, COD values of 171,177.8, and the significant increase in mineral element content. This was mainly because the combination between BHG-I and OPG was more stable, the inhibitory effect was stronger than ICA. Meanwhile, we noticed that the binding between ICA and RANKL (−6.67224169), BMP-2 (−6.69499111), BMP-4 (−6.81634808), Runx2 (−6.87304401)

was the most stable compared with that of BHG-I and IT (**Table 2**). However, the docking scores between BHG-I and the above protein targets were second only to icariin, with the value of −6.09861946, −5.87657118, −6.19196224, and −5.74639988, respectively, which meant BHG-I had good affinity to these bone metabolism proteins (RANKL, BMP-2, BMP-4, Runx-2). The more stable the binding, the less the effect of anti-GIBFI. This accounted for the reason why the anti-GIBFI effect of BHG-I was lower than ICA.

In conclusion, the ligands that bind to OPG, BMP-2, BMP-4, or Runx2 inhibited the differentiation of osteoblasts; the stronger the binding, the more inhibition on the bone formation. The receptors (BMP-2, BMP-4, and Runx2) all combined well to ICA, while BHG-I bound well to OPG; the combination of IT and the above targets was the weakest. IT, BHG-I, and ICA all alleviated bone formation inhibition induced by PNSL, but the order of their intensity in reversing GIBFI was IT>ICA>BHG-I; the most potential compound was found to be IT.

DATA AVAILABILITY STATEMENT

The original contributions presented in the study are included in the article/**Supplementary Material**. Further inquiries can be directed to the corresponding authors.

ETHICS STATEMENT

The animal study was reviewed and approved by the Animal Ethics Committee of Jiangsu University.

AUTHOR CONTRIBUTIONS

All authors listed have made a substantial, direct, and intellectual contribution to the work and approved it for publication.

FUNDING

This work was supported by the National Natural Science Foundation of China (No. 81703773), the Natural Science Foundation of Jiangsu Province (No. BK20170560,), and Jiangsu Science and Technology Development Plan for Chinese Medicine (YB201990).

SUPPLEMENTARY MATERIAL

The Supplementary Material for this article can be found online at: https://www.frontiersin.org/articles/10.3389/fenvs.2021.793527/full#supplementary-material

REFERENCES

Allijn, I. E., Oldenkamp, R., Storm, G., Ragas, A. M. J., and Schiffelers, R. M. (2018). Environmental Impact of Switching from the Synthetic Glucocorticoid Prednisolone to the Natural Alkaloid Berberine. *PloS one* 13, e0199095–15. doi:10.1371/journal.pone.0199095

Apaydin, D. C., Jaramillo, P. A. M., Corradi, L., Cosco, F., Rathjen, F. G., Kammertoens, T., et al. (2020). Early-Life Stress Regulates Cardiac Development through an IL-4-Glucocorticoid Signaling Balance. *Cell Rep* 33, 108404–108419. doi:10.1016/j.celrep.2020.108404

Aslani, S., Abhari, A., Sakhinia, E., Sanajou, D., Rajabi, H., and Rahimzadeh, S. (2019). Interplay between microRNAs and Wnt, Transforming Growth Factor-β, and Bone Morphogenic Protein Signaling Pathways Promote Osteoblastic Differentiation of Mesenchymal Stem Cells. *J. Cel Physiol* 234, 8082–8093. doi:10.1002/jcp.27582

Bruneel, B., Mathä, M., Paesen, R., Ameloot, M., Weninger, W. J., and Huysseune, A. (2015). Imaging the Zebrafish Dentition: from Traditional Approaches to Emerging Technologies. *Zebrafish* 12, 1–10. doi:10.1089/zeb.2014.0980

Castillo-Ramírez, L. A., Ryu, S., and De Marco, R. J. (2019). Active Behaviour during Early Development Shapes Glucocorticoid Reactivity. *Sci. Rep.* 9, 12796–12809. doi:10.1038/s41598-019-49388-3

Cavallin, J. E., Battaglin, W. A., Beihoffer, J., Blackwell, B. R., Bradley, P. M., Cole, A. R., et al. (2021). Effects-Based Monitoring of Bioactive Chemicals Discharged to the Colorado River before and after a Municipal Wastewater Treatment Plant Replacement. *Environ. Sci. Technol.* 55, 974–984. doi:10.1021/acs.est.0c05269

Chen, Q., Li, C., Gong, Z., Chan, E. C. Y., Snyder, S. A., and Lam, S. H. (2017). Common Deregulated Gene Expression Profiles and Morphological Changes in Developing Zebrafish Larvae Exposed to Environmental-Relevant High to Low Concentrations of Glucocorticoids. *Chemosphere* 172, 429–439. doi:10.1016/j.chemosphere.2017.01.036

Cheng, Q., Zhang, X., Jiang, J., Zhao, G., Wang, Y., Xu, Y., et al. (2017). Postmenopausal Iron Overload Exacerbated Bone Loss by Promoting the Degradation of Type I Collagen. *Biomed. Res. Int.* 2017, 1345193–1345202. doi:10.1155/2017/1345193

Chien, S. Y., Tsai, C. H., Liu, S. C., Huang, C. C., Lin, T. H., Yang, Y. Z., et al. (2020). Noggin Inhibits IL-1β and BMP-2 Expression, and Attenuates Cartilage Degeneration and Subchondral Bone Destruction in Experimental Osteoarthritis. *Cells* 9, 1–7. doi:10.3390/cells9040927

DiBattista, J. D., Anisman, H., Whitehead, M., and Gilmour, K. M. (2005). The Effects of Cortisol Administration on Social Status and Brain Monoaminergic Activity in Rainbow troutOncorhynchus Mykiss. *J. Exp. Biol.* 208, 2707–2718. doi:10.1242/jeb.01690

Feng, R., Feng, L., Yuan, Z., Wang, D., Wang, F., Tan, B., et al. (2013). Icariin Protects against Glucocorticoid-Induced Osteoporosis *In Vitro* and Prevents Glucocorticoid-Induced Osteocyte Apoptosis *In Vivo*. *Cell Biochem Biophys* 67, 189–197. doi:10.1007/s12013-013-9533-8

Garg, P., Mazur, M. M., Buck, A. C., Wandtke, M. E., Liu, J., and Ebraheim, N. A. (2017). Prospective Review of Mesenchymal Stem Cells Differentiation into Osteoblasts. *Orthop. Surg.* 9, 13–19. doi:10.1111/os.12304

Goh, S. X. L., Duarah, A., Zhang, L., Snyder, S. A., and Lee, H. K. (2016). Online Solid Phase Extraction with Liquid Chromatography-Tandem Mass Spectrometry for Determination of Estrogens and Glucocorticoids in Water. *J. Chromatogr. A* 1465, 9–19. doi:10.1016/j.chroma.2016.08.040

Hashimi, S. M. (2019). Exogenous Noggin Binds the BMP-2 Receptor and Induces Alkaline Phosphatase Activity in Osteoblasts. *J. Cel Biochem* 120, 13237–13242. doi:10.1002/jcb.28597

Hidasi, A. O., Groh, K. J., Suter, M. J.-F., and Schirmer, K. (2017). Clobetasol Propionate Causes Immunosuppression in Zebrafish (*Danio rerio*) at Environmentally Relevant Concentrations. *Ecotoxicology Environ. Saf.* 138, 16–24. doi:10.1016/j.ecoenv.2016.11.024

Huang, X. Q., Cen, X., Sun, W. T., Xia, K., Yu, L. Y., Liu, J., et al. (2019). CircPOMT1 and circMCM3AP Inhibit Osteogenic Differentiation of Human Adipose-Derived Stem Cells by Targeting miR-6881-3p. *Am. J. Transl Res.* 11, 4776–4788.

Jiang, J., Xiao, S., Xu, X., Ma, H., Feng, C., and Jia, X. (2018). Isomeric Flavonoid Aglycones Derived from Epimedii Folium Exerted Different Intensities in

Anti-osteoporosis through OPG/RANKL Protein Targets. *Int. immunopharmacology* 62, 277–286. doi:10.1016/j.intimp.2018.07.017

Khosla, S. (2001). Minireview: the OPG/RANKL/RANK System. *Endocrinology* 142, 5050–5055. doi:10.1210/endo.142.12.8536

Kišonaitė, M., Wang, X., and Hyvönen, M. (2016). Structure of Gremlin-1 and Analysis of its Interaction with BMP-2. *Biochem. J.* 473, 1593–1604.

Knafo, S., and Wyart, C. (2018). Active Mechanosensory Feedback during Locomotion in the Zebrafish Spinal Cord. *Curr. Opin. Neurobiol.* 52, 48–53. doi:10.1016/j.conb.2018.04.010

Kovács, B., Vajda, E., and Nagy, E. E. (2019). Regulatory Effects and Interactions of the Wnt and OPG-RANKL-RANK Signaling at the Bone-Cartilage Interface in Osteoarthritis. *Int. J. Mol. Sci.* 20, 1–9. doi:10.3390/ijms20184653

Kushlinskii, N. E., Gershtein, E. S., Solov'ev, Y. N., Timofeev, Y. S., Babkina, I. V., Dolinkin, A. O., et al. (2017). Receptor Activator of Nuclear Transcription Factor NF-Kb (RANK), its Ligand RANKL, and Natural Inhibitor of RANKL Osteoprotegerin (OPG) in the Blood Serum of Patients with Primary Bone Tumors. *Bull. Exp. Biol. Med.* 163, 478–481. doi:10.1007/s10517-017-3832-9

Leusch, F. D. L., Neale, P. A., Hebert, A., Scheurer, M., and Schriks, M. C. M. (2017). Analysis of the Sensitivity of *In Vitro* Bioassays for Androgenic, Progestagenic, Glucocorticoid, Thyroid and Estrogenic Activity: Suitability for Drinking and Environmental Waters. *Environ. Int.* 99, 120–130. doi:10.1016/j.envint.2016.12.014

Li, C., Li, Q., Mei, Q., and Lu, T. (2015). Pharmacological Effects and Pharmacokinetic Properties of Icariin, the Major Bioactive Component in Herba Epimedii. *Life Sci.* 126, 57–68. doi:10.1016/j.lfs.2015.01.006

Li, M., Wan, P., Wang, W., Yang, K., Zhang, Y., and Han, Y. (2019). Regulation of Osteogenesis and Osteoclastogenesis by Zoledronic Acid Loaded on Biodegradable Magnesium-Strontium alloy. *Sci. Rep.* 9, 933–943. doi:10.1038/s41598-018-37091-8

Lim, R., Li, L., Chew, N., and Yong, E. L. (2017). The Prenylflavonoid Icaritin Enhances Osteoblast Proliferation and Function by Signal Transducer and Activator of Transcription Factor 3 (STAT-3) Regulation of C-X-C Chemokine Receptor Type 4 (CXCR4) Expression. *Bone* 105, 122–133. doi:10.1016/j.bone.2017.08.028

Lim, Y. J., Kim, K. M., and Jang, W. G. (2021). Chrysophanol Increases Osteoblast Differentiation via AMPK/Smad1/5/9 Phosphorylation *In Vitro* and *In Vivo*. *Clin. Exp. Pharmacol. Physiol.* 48, 515–523. doi:10.1111/1440-1681.13443

Liu, L., Tao, W., Pan, W., Li, L., Yu, Q., Zhang, D., et al. (2018a). Hydroxysafflor Yellow A Promoted Bone Mineralization and Inhibited Bone Resorption Which Reversed Glucocorticoids-Induced Osteoporosis. *Biomed. Res. Int.* 2018, 6762146–6762153. doi:10.1155/2018/6762146

Liu, S., Liu, Y., Jiang, L., Li, Z., Lee, S., Liu, C., et al. (2018b). Recombinant Human BMP-2 Accelerates the Migration of Bone Marrow Mesenchymal Stem Cells via the CDC42/PAK1/LIMK1 Pathway *In Vitro* and *In Vivo*. *Biomater. Sci.* 7, 362–372. doi:10.1039/c8bm00846a

Liu, W., Mao, L., Ji, F., Chen, F., Wang, S., and Xie, Y. (2017). Icariside II Activates EGFR-Akt-Nrf2 Signaling and Protects Osteoblasts from Dexamethasone. *Oncotarget* 8, 2594–2603. doi:10.18632/oncotarget.13732

Liu, W., and Zhang, X. (2015). Receptor Activator of Nuclear Factor-Kb Ligand (RANKL)/RANK/osteoprotegerin System in Bone and Other Tissues (Review). *Mol. Med. Rep.* 11, 3212–3218. doi:10.3892/mmr.2015.3152

Luo, S., Yang, Y., Chen, J., Zhong, Z., Huang, H., Zhang, J., et al. (2016). Tanshinol Stimulates Bone Formation and Attenuates Dexamethasone-Induced Inhibition of Osteogenesis in Larval Zebrafish. *J. orthopaedic translation* 4, 35–45. doi:10.1016/j.jot.2015.07.002

Martella, A., Sepe, R. M., Silvestri, C., Zang, J., Fasano, G., Carnevali, O., et al. (2016). Important Role of Endocannabinoid Signaling in the Development of Functional Vision and Locomotion in Zebrafish. *FASEB J.* 30, 4275–4288. doi:10.1096/fj.201600602r

Martini, A., Huysseune, A., Witten, P. E., and Boglione, C. (2021). Plasticity of the Skeleton and Skeletal Deformities in Zebrafish (*Danio rerio*) Linked to Rearing Density. *J. Fish. Biol.* 98, 971–986. doi:10.1111/jfb.14272

McNeil, P. L., Nebot, C., Cepeda, A., and Sloman, K. A. (2016). Environmental Concentrations of Prednisolone Alter Visually Mediated Responses during Early Life Stages of Zebrafish (*Danio rerio*). *Environ. Pollut.* 218, 981–987. doi:10.1016/j.envpol.2016.08.048

Neale, P. A., Grimaldi, M., Boulahtouf, A., Leusch, F. D. L., and Balaguer, P. (2020). Assessing Species-specific Differences for Nuclear Receptor Activation for Environmental Water Extracts. *Water Res.* 185, 116247–116312. doi:10.1016/j.watres.2020.116247

Nesan, D., Kamkar, M., Burrows, J., Scott, I. C., Marsden, M., and Vijayan, M. M. (2012). Glucocorticoid Receptor Signaling Is Essential for Mesoderm Formation and Muscle Development in Zebrafish. *Endocrinology* 153, 1288–1300. doi:10.1210/en.2011-1559

Nunes, M. E. M., Schimith, L. E., Costa-Silva, D. G., Leandro, L. P., Martins, I. K., De Mello, R. S., et al. (2020). Acute Embryonic Exposure of Zebrafish to Permethrin Induces Behavioral Changes Related to Anxiety and Aggressiveness in Adulthood. *J. Psychiatr. Res.* 121, 91–100. doi:10.1016/j.jpsychires.2019.11.006

Øverli, Ø., Kotzian, S., and Winberg, S. (2002). Effects of Cortisol on Aggression and Locomotor Activity in Rainbow trout. *Horm. Behav.* 42, 53–61. doi:10.1006/hbeh.2002.1796

Pedrouzo, M., Borrull, F., Marcé, R. M., and Pocurull, E. (2009). Ultra-high-performance Liquid Chromatography-Tandem Mass Spectrometry for Determining the Presence of Eleven Personal Care Products in Surface and Wastewaters. *J. Chromatogr. A* 1216, 6994–7000. doi:10.1016/j.chroma.2009.08.039

Pitt, J. A., Kozal, J. S., Jayasundara, N., Massarsky, A., Trevisan, R., Geitner, N., et al. (2018). Uptake, Tissue Distribution, and Toxicity of Polystyrene Nanoparticles in Developing Zebrafish (*Danio rerio*). *Aquat. Toxicol.* 194, 185–194. doi:10.1016/j.aquatox.2017.11.017

Schmid, S., Willi, R. A., Salgueiro-González, N., and Fent, K. (2020b). Effects of New Generation Progestins, Including as Mixtures and in Combination with Other Classes of Steroid Hormones, on Zebrafish Early Life Stages. *Sci. Total Environ.* 709, 136262–136312. doi:10.1016/j.scitotenv.2019.136262

Schmid, S., Willi, R. A., and Fent, K. (2020a). Effects of Environmental Steroid Mixtures Are Regulated by Individual Steroid Receptor Signaling. *Aquat. Toxicol.* 226, 105562–105571. doi:10.1016/j.aquatox.2020.105562

Silvério de Barros, R., Dias, G. S., Paula do Rosario, A., Paladino, F. V., Lopes, G. H., and Campos, A. H. (2019). Gremlin-1 Potentiates the Dedifferentiation of VSMC in Early Stages of Atherosclerosis. *Differentiation* 109, 28–33. doi:10.1016/j.diff.2019.08.001

Sun, E., Xu, F., Qian, Q., Cui, L., Tan, X., and Jia, X. (2016). Metabolite Profiles of Icariin in Rat Feces, Bile and Urine by Ultraperformance Liquid-Chromatography/Quadrupole-Time-Of-Flight Mass Spectrometry. *J. Chromatogr. Sci.* 54, 158–164. doi:10.1093/chromsci/bmv121

Sun, E., Xu, F., Qian, Q., Cui, L., Tan, X., and Jia, X. (2014). Ultra-performance Liquid Chromatography/quadrupole-Time-Of-Flight Mass Spectrometry Analysis of Icariside II Metabolites in Rats. *Nat. Product. Res.* 28, 1525–1529. doi:10.1080/14786419.2014.921684

Tekari, A., May, R. D., May, R., Frauchiger, D., Chan, S., Benneker, L., et al. (2017). The BMP2 Variant L51P Restores the Osteogenic Differentiation of Human Mesenchymal Stromal Cells in the Presence of Intervertebral Disc Cells. *Eur. Cell Mater.* 33, 197–210. doi:10.22203/ecm.v033a15

Tyrovola, J. B., and Odont, X. (2015). The "Mechanostat Theory" of Frost and the OPG/RANKL/RANK System. *J. Cel. Biochem.* 116, 2724–2729. doi:10.1002/jcb.25265

Varga, Z. M., Ekker, S. C., and Lawrence, C. (2018). Workshop Report: Zebrafish and Other Fish Models-Description of Extrinsic Environmental Factors for Rigorous Experiments and Reproducible Results. *Zebrafish* 15, 533–535. doi:10.1089/zeb.2018.29006.zol

Vimalraj, S., Saravanan, S., Hariprabu, G., Yuvashree, R., Ajieth Kanna, S. K., Sujoy, K., et al. (2020). Kaempferol-Zinc(II) Complex Synthesis and Evaluation of Bone Formation Using Zebrafish Model. *Life Sci.* 256, 117993–118006. doi:10.1016/j.lfs.2020.117993

Wang, Z., Wang, D., Yang, D., Zhen, W., Zhang, J., and Peng, S. (2018). The Effect of Icariin on Bone Metabolism and its Potential Clinical Application. *Osteoporos. Int.* 29, 535–544. doi:10.1007/s00198-017-4255-1

Willi, R. A., Faltermann, S., Hettich, T., and Fent, K. (2018). Active Glucocorticoids Have a Range of Important Adverse Developmental and Physiological Effects on Developing Zebrafish Embryos. *Environ. Sci. Technol.* 52, 877–885. doi:10.1021/acs.est.7b06057

Willi, R. A., Salgueiro-González, N., Carcaiso, G., and Fent, K. (2019). Glucocorticoid Mixtures of Fluticasone Propionate, Triamcinolone Acetonide and Clobetasol Propionate Induce Additive Effects in Zebrafish Embryos. *J. Hazard. Mater.* 374, 101–109. doi:10.1016/j.jhazmat.2019.04.023

Wilson, K. S., Matrone, G., Livingstone, D. E. W., Al-Dujaili, E. A. S., Mullins, J. J., Tucker, C. S., et al. (2013). Physiological Roles of Glucocorticoids during Early Embryonic Development of the Zebrafish (*Danio rerio*). *J. Physiol.* 591, 6209–6220. doi:10.1113/jphysiol.2013.256826

Wolter, M. E., and Svoboda, K. R. (2020). Doing the Locomotion: Insights and Potential Pitfalls Associated with Using Locomotor Activity as a Readout of the Circadian Rhythm in Larval Zebrafish. *J. Neurosci. Methods* 330, 108465–108519. doi:10.1016/j.jneumeth.2019.108465

Yang, H., Guo, Y., Wang, D., Yang, X., and Ha, C. (2018). Effect of TAK1 on Osteogenic Differentiation of Mesenchymal Stem Cells by Regulating BMP-2 via Wnt/β-Catenin and MAPK Pathway. *Organogenesis* 14, 36–45. doi:10.1080/15476278.2018.1455010

Zhang, H., Wang, H., Wei, J., Chen, X., Sun, M., Ouyang, H., et al. (2018). Comparison of the Active Compositions between Raw and Processed Epimedium from Different Species. *Molecules* 23, 1–7. doi:10.3390/molecules23071656

Zhao, Y., Wang, H.-L., Li, T.-T., Yang, F., and Tzeng, C.-M. (2020). Baicalin Ameliorates Dexamethasone-Induced Osteoporosis by Regulation of the RANK/RANKL/OPG Signaling Pathway. *Drug Des. Dev. Ther.* 14, 195–206. doi:10.2147/dddt.s225516

Zhao, Y., Zhang, K., and Fent, K. (2016). Corticosteroid Fludrocortisone Acetate Targets Multiple End Points in Zebrafish (*Danio rerio*) at Low Concentrations. *Environ. Sci. Technol.* 50, 10245–10254. doi:10.1021/acs.est.6b03436

Zhao, Y., Zhang, K., and Fent, K. (2018). Regulation of Zebrafish (*Danio rerio*) Locomotor Behavior and Circadian Rhythm Network by Environmental Steroid Hormones. *Environ. Pollut.* 232, 422–429. doi:10.1016/j.envpol.2017.09.057

Zheng, S., Huang, W., Liu, C., Xiao, J., Wu, R., Wang, X., et al. (2021). Behavioral Change and Transcriptomics Reveal the Effects of 2, 2', 4, 4'-tetrabromodiphenyl Ether Exposure on Neurodevelopmental Toxicity to Zebrafish (*Danio rerio*) in Early Life Stage. *Sci. Total Environ.* 752, 141783–142152. doi:10.1016/j.scitotenv.2020.141783

Zwart, N., Jonker, W., Broek, R. T., de Boer, J., Somsen, G., Kool, J., et al. (2020). Identification of Mutagenic and Endocrine Disrupting Compounds in Surface Water and Wastewater Treatment Plant Effluents Using High-Resolution Effect-Directed Analysis. *Water Res.* 168, 115204–115234. doi:10.1016/j.watres.2019.115204

Conflict of Interest: The authors declare that the research was conducted in the absence of any commercial or financial relationships that could be construed as a potential conflict of interest.

Publisher's Note: All claims expressed in this article are solely those of the authors and do not necessarily represent those of their affiliated organizations, or those of the publisher, the editors, and the reviewers. Any product that may be evaluated in this article, or claim that may be made by its manufacturer, is not guaranteed or endorsed by the publisher.